EULERIAN-LAGRANGIAN COUPLING FOR HELICOPTER ROTOR AERODYNAMICS

B. Rodriguez, R. Boisard
Onera – The French Aerospace Lab
F-92190, Meudon, France

J. Mayeur
Onera – The French Aerospace Lab
F-92320, Châtillon, France

Abstract

This article presents a new hybrid methodology which couples a free wake model with a CFD code in the context of CSD/CFD simulation. The coupling strategy is detailed, especially the treatment used to combine the different time scales used in the Eulerian and in the Lagrangian models. Validation of the methodology on two different tests case is presented. The first one validates the methodology for a high speed flight. The second one exhibits the ability of this hybrid method to capture the BVI events with an accuracy equivalent to the CFD code.

NOTATION

a_∞	Free stream sound speed, m/s
ρ_∞	Free stream density, kg/m^3
V_∞	Free stream velocity, m/s
M_∞	Free stream Mach number
M_{tip}	Rotor tip Mach number
μ	Advancing ratio, M_∞/M_{tip}
ω	Rotor rotation velocity, rd/s
R	Blade radius, m
r	Spanwise location, m
c	Blade chord, m
S	Rotor disk area, m^2
σ	Rotor solidity, $\frac{bcR}{\pi R^2}$, b number of blades
T	Rotor lift, N
$\overline{Z}$	Non dimensional lift, $\frac{100T}{\frac{1}{2}\rho(\omega R)^2 S\sigma}$
C_x	Drag coefficient
R_e	Reynolds number (based on c and V_∞)
α_q	Shaft angle, deg
r_c	vortex core radius, m
φ	Azimuth, deg
Γ	Circulation, m^2/s
C_nM^2	Sectional normal force coefficient
C_mM^2	Sectional pitching moment coefficient

1. INTRODUCTION

Rotorcraft configurations involve complex vortex flows generated by the rotor mainly at the blade tip. First of all, the velocities induced by this vorticity field are the sources of the induced power, a component of the rotor power dominating at low speed. These induced velocities contribute to unsteady modifications of the sectional blade loads which lead to structural vibrations. The most impulsive ones are also sources of the noise radiated as in the strong blade-vortex interactions (BVI) events.

Eulerian methods are generally used to compute the unsteady flow field around the rotor with a particular ability to simulate the near-body field. Their main weakness is their dissipative behaviour. Mesh refinement is the simplest solution to solve it but with a high CPU cost. For the simulation of the BVI events different approaches can be used to achieve the capture of the vortex flow with limited CPU requirements such as adaptative refinement, high order scheme or adapted grids [1][2][3].

On the contrary, Lagrangian methods have the ability to preserve the vortex source term of the flow field solving the vorticity transport equation[6], or by the transport of the vortex strength itself in the case of classical wake models. Nevertheless, these methods often lack the ability to accurately compute the 3D transonic viscous aerodynamics near the rotor blade, especially in the case of a wake model using a lifting line approach to model the blade.

Several works have been done to couple these two approaches and use the best part of each one, Eulerian method for the near body field and Lagrangian method for the wake. In the work detailed in [5], a coupling is performed between a Navier-Stokes/Full Potential domain and a free-wake model which is only used to correct the far field condition. In [7], an interface is developed between the free wake model MESIR and a full-potential code FP3D. The free wake induced velocity is considered as a perturbation on the blade surface. Recently Viscous Vortex Particle

model has been coupled with a CFD model in a CSD/CFD coupling context[6]. Accurate results have been presented but the CPU time reduction compare to the full CFD computation is limited due to the cost of the VVPM model.
In the present paper, the coupling between a free wake model, with low CPU requirement, and an Eulerian code is detailed in the context of a CSD/CFD loose coupling. This methodology allows the simulation of only one blade in the CFD code with a reduced near-body mesh while all the blades are used in the free wake model.
The accuracy of the hybrid method is compared to the full CFD method and to the experimental results for an advancing flight configuration with transonic phenomena and a descending flight configuration with BVI events.

2. METHOD

2.1. Eulerian model

The Eulerian *elsA* solver, developed by ONERA since 1997, is used to solve the near body aerodynamic field. This multi-application object oriented aerodynamic code is based on a cell-centred finite volume formulation for structured meshes. Solving the Euler or the Reynolds Averaged Navier-Stokes equations, it allows to simulate a wide range of aerospace configurations such as aircraft, space launchers, turbomachinery, missile configurations and helicopters.
The space discretization is based on the classical 2nd order centred Jameson's scheme employed with a scalar artificial viscosity and Martinelli's correction.
Several time discretization schemes are available to compute the unsteady computations. Explicit or implicit schemes, such as a pseudo-time approach (Dual Time Stepping) or the Gear method, are available. The time integration can be solved either by an implicit residual smoothing phase with a 4th order Runge–Kutta technique or by an implicit LU scalar relaxation phase associated to a backward Euler scheme. In the present paper, the Gear method is used to perform all the computations.
The *elsA* solver contains many turbulence models. The turbulent computations presented in this paper use the two-equation Wilcox k-ω model with the Zheng limiter and a SST correction.

2.2. Lagrangian model

The Lagrangian model includes a lifting line model and a potential wake model. The Lagrangian region is computed inside the HOST [9] code. This comprehensive dynamic code was developed by Eurocopter France in order to simulate and analyze the behaviour of an isolated rotor or a complete helicopter in various flight conditions.
Several wake models are available in the HOST code. They are all based on a Lagrangian approach.
The simplest one is the METAR prescribed wake model. The helicoïdal wake growing depends on the far field velocity and the mean induced velocity. The METAR wake is decritized by lattices in the spanwise direction and in the azimuthal direction (Figure 1). The radial lattices carry the radial gradient of circulation; the azimuthal lattices transport the time gradient of the circulation. The circulation in the wake induces a velocity field which is computed by the Biot and Savart law. For a lattice, the analytical formula has a singularity in 1/r which needs to be regularized. A regularization formulation based on the Scully vortex model is used.
Another wake model available in the HOST code is the MESIR [10] wake model. It is a periodic free-wake model. The discretization is the same as the METAR model. The geometry of the wake is free but the kinematics of the wake follows a periodic movement and is converged with an iterative process. Figure 2 shows a view of the MESIR wake geometry for the HARTII [11] baseline test case.
These two models are limited to stabilized flight conditions. Due to numerical instability of these wake models, the computational time step is rarely reduced below 10° of azimuth. Nevertheless, this is not a limitation for their classical use in the context of a comprehensive dynamic code.
The wake model MINT [12] is also available in the HOST code. This wake model is an unsteady free wake model without any periodic assumption. The high order modelisation of the wake increases the numerical stability and accuracy of simulation. Computations with a reduced time step can be achieved [13]. Nevertheless, for stabilized flight conditions, METAR or MESIR are sufficients.

2.3. Coupling strategy

2.3.1. *elsA* interface

The *elsA* code already provides a python interface with the ability to exchange data as input or output during the computation with a CGNS/Python representation. In the present work, the exterior state of the non reflection condition applied at the outer boundary of the blade mesh (Figure 4) is modified at each node during the iteration thanks to a CGNS/Python structure provided in memory to the *elsA* code.

2.3.2. Wake model interface

A specific python module is developed for the HOST code.
This module is based on Python/C/Fortran architecture using the Numpy [14] C-API to exchange memory buffer

between the different language layers. This module is called in a script executed by the HOST code using the Python [15] C/API. The memory context being the same between this module and the HOST code, it can access the wake model data such as the geometry and the circulation at each time step.
This module computes the velocities induced by the wake on a prescribed mesh. An OpenMP parallelization on the receivers is performed for the computation of the induced velocities to reduce the CPU time.
This Python module interface uses the CGNS/Python representation in order to be compliant with the *elsA* interface dataflow.
Figure 3 presents a view of the MESIR wake with the induced velocities computed in a plane in the rotor wake. The streamlines identify the two main vortex structures of the wake.

2.3.3. Coupling loop

Figure 4 presents the scheme of the coupling method. For the current work, the coupling is performed in the loop of a loose coupling[18][19] and the exchanges are performed by files. Nevertheless, the interfaces of the Eulerian and the Lagrangian models are designed to permit exchange on network using for example the classical Python network libraries. The outer boundaries points of the Eulerian mesh are provided to the Lagrangian model for a rotor revolution. In return, the Lagrangian model computes the velocities induced by the lifting lines and the wake model on the mesh points for the complete period.
The Euler/Lagrange coupling is performed in a loose coupling procedure where the CFD loads and the blades kinematics are exchange between the Eulerian code and the comprehensive dynamic code. At convergence of the loose coupling, the CFD loads replace totally the comprehensive dynamic code aerodynamic loads. The circulation used in the wake model is totally coherent with the CFD loads and so is the induced velocity.

2.3.4. Timescale

In the current coupling, there are no needs for a coherency between the time step in the CFD model and the time step in the Lagrangian model. On the *elsA* side, the outer conditions are provided by the Lagrangian model for a complete revolution with a fixed time step. The Python module which pre-processes the data for *elsA* performs a linear interpolation or a Fourier interpolation to conform the input data to the *elsA* time step. Nevertheless, this interpolation does not improve the frequency content of the data provided to the *elsA* code by the Lagrangian model.

On the Lagrangian side, the wake model (METAR, MESIR) is solved using a time step greater or equal to 10° due to numerical stability considerations. If the induced velocities are computed with this time sampling, the frequency content provides to the *elsA* code will not be sufficient to transfer the vortex structure.

In fact, considering a vortex interacting with a blade (Figure 6), depending on the blade azimuth and the radial station, the convecting velocity of the vortex could be simply modelised in the airfoil frame. The translation of the vortex relatively to the outer boundaries of the blade mesh depends on the time step and on its convecting velocity (Figure 6). With a length wave of the vortex equivalent to its core diameter, its sampling should be greater than 2 points in this wave period. The following equation gives the azimuthal step required to have a translation distance of the vortex equal to 2 radii between two instants of computation of the induced velocity on the outer boundary of the CFD mesh:

$$(1) \quad \delta\varphi = \frac{2\, r_c / R}{r / R \pm \mu}$$

+/-: respectively advancing or retreating side

Figure 7 shows a spanwise distribution of this equation for a vortex radius of 15% or 20% of chord on HARTII blade. The lower vortex radius corresponds to the measurement obtained during the HARTII campaign[16] close the blade interaction location. An azimuth step of 1° ensures that the vortex is at least discretized by two steps in the induced velocity conditions provided to the Eulerian code. It is clear that for configurations with strong blade vortex interaction the time step of the vortex sampling has to be carefully chosen.

The core radius of the tip vortex modelised by the MESIR can be estimated. Figure 8 shows the component along the Z axis of the velocity induced by the MESIR wake on a plane intersecting the blade tip vortex modelised by the roll-up of several lattices. This component of velocity is plotted along horizontal lines in Figure 8. A rough vortex structure can be noticed. A core radius is estimated which corresponds to 40% of chord. The plane is not totally normal to the vortex axis. This core radius is certainly over estimated but this value confirms that a time step of 1° used for the sampling of the induced velocity should be sufficient.

The Lagrangian wake is solved with an azimuthal step of 10°. Following the above discussion, to ensure a sufficient sampling of the boundary conditions provided to the *elsA* code, an interpolation in time of the wake variables coordinates and circulation is performed to obtain the vortices positions for a time step reduced to 1°. This treatment allows a MESIR computation with a time step of 10° with a good transfer of the vortex structure to the CFD code.

2.3.5. CPU cost

Compared to a full CFD computation, the hybrid method has a reduced CFD domain with no background grid. The very fine background grid usually seen in classical BVI computation is no longer needed. The main CPU cost of the Lagrangian method is the computation of the induced velocities on the boundaries of the CFD mesh, but it is several orders of magnitude lower than the CPU cost of the CFD computation on the background grid. Despite the fact that the gain in CPU time is clear, it will depend on the refinement of the full CFD computation used as reference.

3. RESULTS

3.1. Advancing operating flight

3.1.1. Test case

The test case is the experimental configuration 1.2 F1 of the 7A rotor in advancing flight realized during the 11th campaign in S1MA wind tunnel (ONERA, France 1991). The test case flow conditions and main geometric characteristics are defined in Table 1. The unsteady pressures on the blades were measured with Kulites along the chord at five spanwise locations (r/R=0.5, 0.7, 0.825, 0.915, 0.975). From the unsteady pressures, the sectional moments and loads are computed in the local airfoil frame (leading edge to trailing edge).

Test case 1.2 F1	
μ	0.4
M_{tip}	0.646
$\overline{Z}$	12.5
$(C_x S)_f / S\sigma$	0.1
Flow conditions	
V_∞	89 m/s
Re	$3.1\ 10^6$
α_q	-13.75°
Geometric characteristics	
R	2.1 m
c	0.140 m

Table 1 - Experiment characteristics

During the experiment, the blade deformation is also measured using the strain gauges and the Strain Pattern Analysis (SPA) method [2]. The post-processing of the measurements provides the lead-lag, the torsion and flapping along the spanwise depending on the azimuth.

3.1.2. Numerical configuration

3.1.2.1. Eulerian region

On the Eulerian side, the near body mesh of the blade is a structured grid with O topology. Figure 9 shows the surface mesh at the blade tip and the multiblock topology of the grid. The blade grid contains 18 blocks with 3 Million nodes and a normal extension equivalent to 1 blade chord.

For the reference computation with the full *elsA* code, the off body mesh is a Cartesian grid generated by an Octree space decomposition strategy [20]. Figure 9 presents a view of the Cartesian mesh with the 4 near body meshes. The background grid contains 165 blocks with 40 Millions nodes. Not matching connectivities are used between the different levels of the Cartesian mesh.

The *elsA* computation is performed with a viscous and turbulent assumption. The turbulent model is the k-ω Wilcox model with a Zheng limiter and a SST correction. The spatial discretization is the Jameson scheme with a scalar artificial viscosity and a Martinelli correction. The time scheme is a Backward Euler with Gear sub-iteration. LU decomposition is used with SSOR relaxation.

The *Ael* module[21] of the *elsA* software is used for the deformation of the mesh depending on the blades kinematics provided by the HOST code.

3.1.2.2. Lagrangian region

In HOST, the MESIR wake model is used with a time step equivalent to 10°. The coupling data are exchanged with a time step of 1°.

3.1.3. Results

Figure 10 shows a comparison of the sectional normal load at different radial stations between the experiment, the computation full *elsA* and the hybrid computation. The two numerical results are very close with the same trends. Slight differences are located between 0° and 80° and at 100° and 180° azimuth. For the azimuth 100° and 180° the peaks of load are slightly better predicted with the pure Eulerian method.

For the sectional pitching moment presented in Figure 11, the results obtain by the two numerical methods are very close until r/R=0.7. For the radial stations r/R=0.825 and r/R=0.975, as for the normal force, the main difference appears around 100° azimuth at the negative peak. The negative peak of pitching moment is better predicted by the pure Eulerian method especially at r/R=0.825. It should be investigated if this difference is due to a lack of modelisation of the wake in the hybrid method. Nevertheless, compared to the experiment, the hybrid results have a behaviour equivalent to the classical method.

3.2. Descent operating flight
3.2.1. Test case

The test case considered is the HART II baseline test case[11] with strong blade-vortex interactions (BVI). The HART II experimental campaign was conducted in the DNW German-Dutch wind tunnel. Active participants of NASA Langley, US Army Aeroflightdynamics Directorate (AFDD), DLR, DNW and ONERA contribute to the Workshop.
The rotor is a fully instrumented Bo-105 model rotor, 4m in diameter, equipped with four hingeless blades, which have a pre-cone angle of 2.5°. The blades are rectangular with -8°/R of linear twist, and they are equipped with modified NACA23012 airfoil, with a chord length of 0.121 m.
The experimental conditions are summarized in Table 2 .

HARTII - Baseline	
ω	109.01 rd/s
μ	0.15
M_{tip}	0.641
α_q	4.5°
Geometric characteristics	
R	2 m
c	0.121 m

Table 2 - Experiment characteristics

Several measurements were performed during the experiments. The 3-Components Particule Image Velocimetry technique is used to identified vortex wake locations and vortex characteristics [16]. Balances are used to measure the rotor loads. Kulite sensors measured the unsteady pressure on various sections. Only one has a sufficient distribution of measurement to compute the sectional loads by integration assuming a constant piecewise pressure distribution[17]. The conditional average of the unsteady sectional loading is used in the present paper comparisons. The blade position and deformation are measured using the Stereo Pattern Recognitions (SPR).

3.2.2. Numerical configuration
3.2.2.1. Eulerian region

On the Eulerian side, as for the 7A rotor computation, the near body grid has an O topology. The computation is performed with a non viscous assumption. The near body grid contains 570 000 nodes. For the full *elsA* computation used as reference, the Cartesian background grid contains 38 Million nodes with a grid spacing in the finest mesh level equivalent to 6% of chord.

3.2.2.2. Lagrangian region

In HOST, as for the 7A rotor computation, the MESIR wake model is used with a time step equivalent to 10°. The coupling data are exchanged with a time step of 1°.

3.3. Results

Figure 12 compares the sectional normal force at r/R=0.87 computed by the Euler/Lagrange methodology with different sampling of the boundary conditions and different time steps with the experiment. With an Eulerian time step of 1 deg, if the boundaries conditions sampling is 10 deg no BVI interactions are captured on the advancing or retreating blade sides. With induced velocities computed at the boundary conditions every 1 deg, the BVI interactions appear clearly on the advancing and retreating blade sides. It confirms the importance of the sampling on the Eulerian boundary conditions of the vortices computed in the Lagrangian model. Nevertheless, the lower frequency components are the same with boundary conditions computed every 1° or 10°. Reducing the Eulerian time step from 1° to 0.3° does not seem to improve the BVI interaction predictions. The derivative of the sectional load which are more meaningful from an acoustic point of view, are compared for the different time steps in Figure 13. On the advancing blade side, reducing the time step from 1° to 0.3° slightly improves the amplitude and the phase of the derivative of the sectional normal force. On the retreating blade side, the amplitude is also improved especially at the main experimental peak at 305° azimuth. But the phase is slightly deprecated.
For the time step equivalent to 0.3° of azimuth, in Figure 14, the sectional loads are compared between the full *elsA* computation and the hybrid computation. The full *elsA* computation shows BVI interactions with a higher amplitude on both the advancing and retreating blade sides. The lower frequencies of the sectional load seem to be better predicted in the Eulerian/Lagrangian computation especially around 115° of azimuth. The comparison of the derivative of the sectional loads in Figure 15 shows on the advancing side higher amplitude for the full *elsA* computation but better phase for the *elsA*/MESIR computation. On the retreating side, the behaviour is opposite. The amplitude is better predicted by the

elsA/MESIR methodology but the phase is well predicted by the full *elsA* computation.

For the elsA/MESIR methodology, a Navier-Stokes computation is performed. The sectional loads are compared with the non viscous computation in Figure 16. The amplitude of the BVI interactions is close on the advancing side and slightly reduced on the retreating side. The mean level of the sectional loads is higher on the advancing side around 50° of azimuth and on the retreating side at 250° of azimuth.

For this BVI configuration, the hybrid method achieves accurate results compared to the full *elsA* computation. The slight discrepancy observed may be improved by reducing the time step used for the computation of the boundaries conditions.

4. CONCLUSION

A hybrid methodology designed to reduce the CPU requirements for the rotorcraft aerodynamics computation has been developed in a CFD/CSD context.

Its ability to compute high speed configuration and BVI configuration with accuracy on the sectional loads close to a full CFD code has been demonstrated.

A procedure has been defined to ensure a sufficient transfer of the vortex structure from the Lagrangian model to the Eulerian region.

The validation of the method will be pursued with an acoustic post-processing of the results for the descending configuration.

For the advancing operating flight, the future work will be dedicated to the comparison of rotor performance and the blade kinematics obtained by each methodology.

It is also planed to extend the hybrid methodology to the use of a fully unsteady free wake model which should permit the simulation of maneuvers.

ACKNOWLEDGMENTS

This work was completed in the frame of the SHANEL project funded by French Ministry of Transport (DGAC) and monitored by Ministry of Defence (DGA). The authors want to acknowledge the Eurocopter Company for the financial support which permits to initiate this work, and his colleagues from Onera, especially Dr M. Costes, for all the fruitful technical discussions.

REFERENCES

[1] Boyd D, “HART-II Acoustic Predictions using a Coupled CFD/CSD Method”, American Helicopter Society, 65th Annual Forum, Gravepine, 2009

[2] Dietz M., Keβler M., Krämer E., Wagner S., “Tip Vortex Conservation on a Helicopter Main Rotor Using Vortex-Adapted Chimera Grids”, AIAA Journal , Vol. 45, No. 8, 2007

[3] Renaud T., Perez G., Benoit C., Jeanfaivre G., Péron S., “Blade-Vortex interaction capture by CFD”, 34th European Rotorcraft Forum, Liverpool, 2008

[4] Brown R., “Rotor Wake Modeling for the Flight Dynamic Simulation of Helicopters”, AIAA Journal, Vol. 38, No. 1, January 2000

[5] Berkman E., Sankar L., Berezin C., Torok M., “Navier-Stokes/Full Potential/Free-Wake Method for Rotor Flow”, Journal of Aircraft, Vol 34, No. 5, September-October 1997.

[6] Zhao J., He C., “Coupled CSD/CFD and Viscous Vortex Particle Method for Rotorcraft comprehensive Analysis”, American Helicopter Society, 68th Annual Forum, Fort Worth, Texas, 2012.

[7] Jobard N., Costes M., Beaumier P., “Three dimensional BVI simulation on Aeroelastic Blades Using a New Deforming Grid Approach Coupled to a Free-Wake Analysis”, 52nd Annual Forum of the American Helicopter Society, Washington, June 1996.

[8] Cambier L., Veuillot J.-P., “Status of the elsA CFD Software for Flow Simulation and Multidisciplinary Applications”, 46th AIAA Aerospace Sciences Meeting and Exhibit, No. 2008-664, Reno, Nevada, USA, January 2008.

[9] Benoit B., Dequin A-M., Kampa K., Grunhagen W., Basset P-M., “HOST: a General Helicopter Tool for Germany and France”, 56th Annual Forum of the American Helicopter Society, Virginia Beach, May 2000.

[10] Michéa B., "Etude des sillages de rotors d'hélicoptère en vol d'avancement et de leur influence sur les performances du rotor", Thèse de doctorat, Université Paris VI, Septembre 2002.

[11] Van der Wall, B.G., “A Comprehensive Rotary-Wing Database for Code Validation: The HART II International Workshop”, The Aeronautical Journal of The Royal Aeronautical Society, Vol. 115, No. 1163, January 2011, pp 91-102; erratum in Vol 115., No. 1166, April 2011, p. 220.

[12] Lebouar G., Costes M., Leroy-Chesneau A., Devinant P., “Numerical simulations of unsteady aerodynamics of helicopter rotor in maneuvering flight conditions”, Aerospace Science and Technology, vol. 8, pp. 11-25, 2004.

[13] Rodriguez B., “Blade Vortex Interaction and Vortex Ring State captured by a fully time marching unsteady wake model coupled with a comprehensive dynamics code”, HeliJapan, Saitama, Japan, November 2010
[14] Jones E., Oliphant T., Peterson P. and others, “SciPy: Open Source Scientific Tools for Python”, 2001 -, http://www.scipy.org
[15] van Rossum G, Drake F.L., Python Reference Manual, PythonLabs, Virginia, USA, 2001. Available at http://www.python.org
[16] Bailly J., Delrieux Y., Beaumier P., “HARTII: Experimental Analysis and Validation of ONERA Methodology for the Prediction of Blade-Vortex Interaction”, 30th European Rotorcarf Forum, Marseille, September 2004.
[17] van der Wall B.G., “2nd HHC Aeroacoustic Rotor Test (HART-II) – Part 1: Test Documentation”, German Aerospace Center Institute Report IB 111-2003/31, November 3, 2003.
[18] Beaumier P., Costes M., Rodriguez B., Poinot M., Cantaloube B, “Weak and strong coupling between the elsA CFD solver and the HOST helicopter comprehensive analysis”, 31st European Rotorcraft Forum, Florence, 2005
[19] Servera G., Beaumier P., Costes M., “A weak coupling method between the dynamics code HOST and the 3D unsteady Euler code WAVES”, Aerospace Science and technology, volume 5, n° 6, septembre 2001, p. 397-408
[20] Péron S., Benoit. C, “Automatic off-body overset adaptive Cartesian mesh method based on an octree approach”, 6th AIAA Theoretical Fluid Mechanics - 20th AIAA Computational Fluid Dynamics Conference, Honolulu, 27-30 juin 2011
[21] Dugeai A., “Aeroelastic Developments in the elsA Code and Unsteady RANS Applications”, International Forum of Aeroelasticity and Structural Dynamics, Munich, July 2005

FIGURES

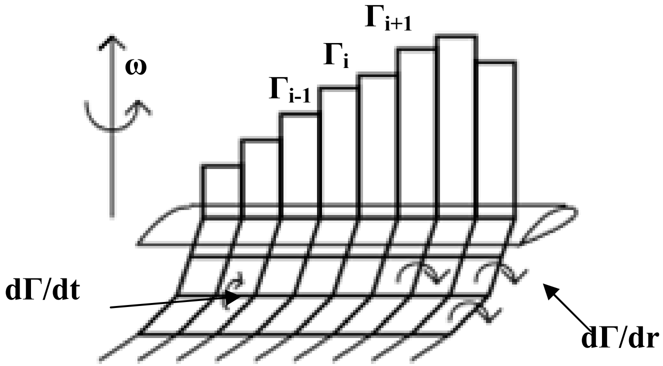

Figure 1 – Scheme of the circulation on the lifting line and in the wake of the METAR model

Figure 2 – MESIR wake geometry – descending flight – HART II BL test case

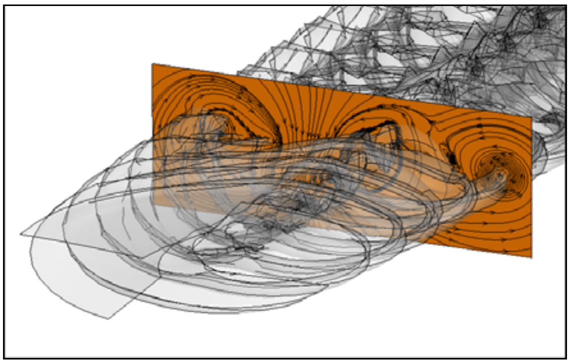

Figure 3 – MESIR wake geometry and induced velocity streamlines in a plane – 7A rotor in advancing flight

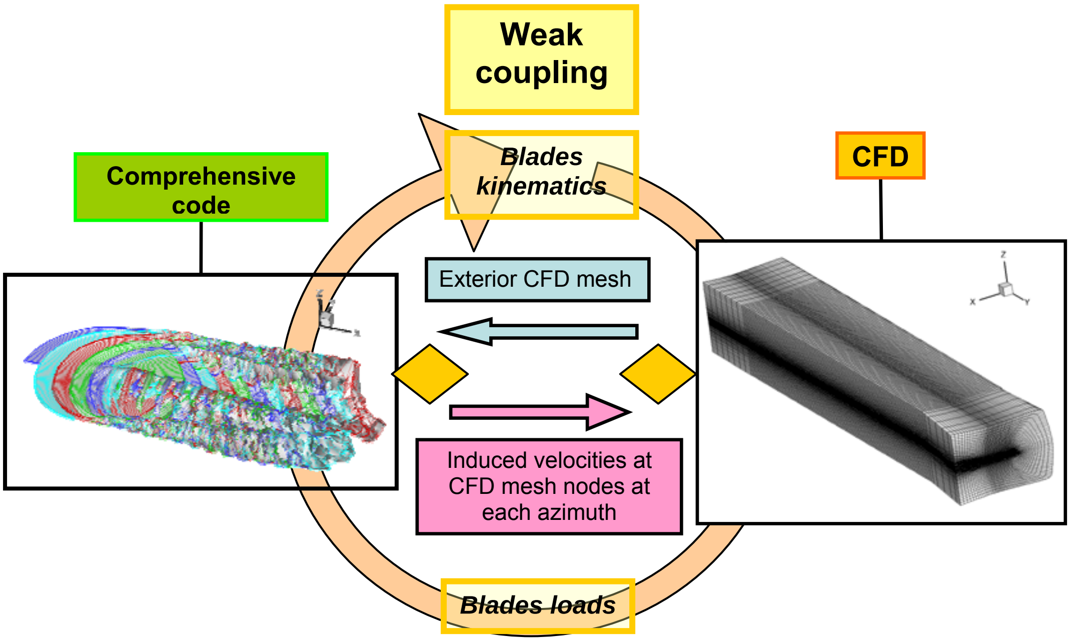

Figure 4 – Coupling procedure

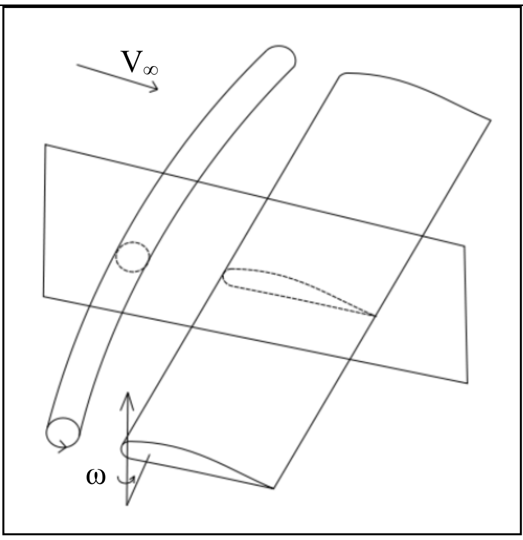

Figure 5 – Scheme of the parallel interaction between a tip vortex tube and a blade

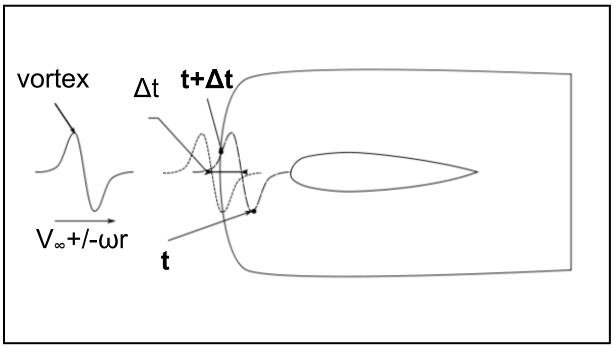

Figure 6 – Sampling of the vortex on the outer boundary of the CFD mesh

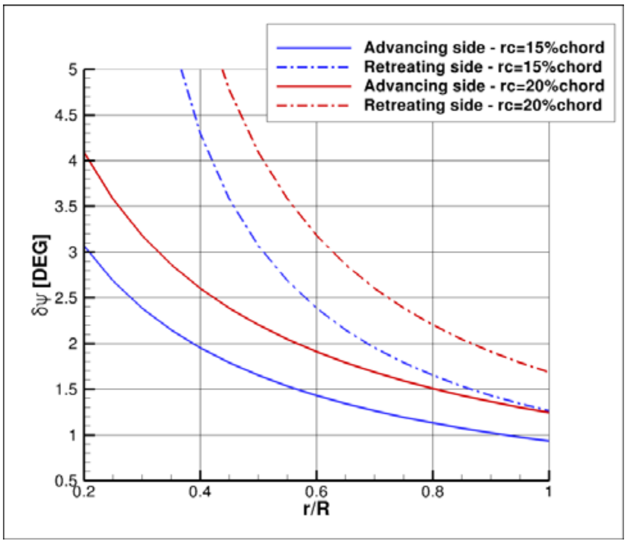

Figure 7 – Azimuthal length of the vortex diameter depending on the blade radial station

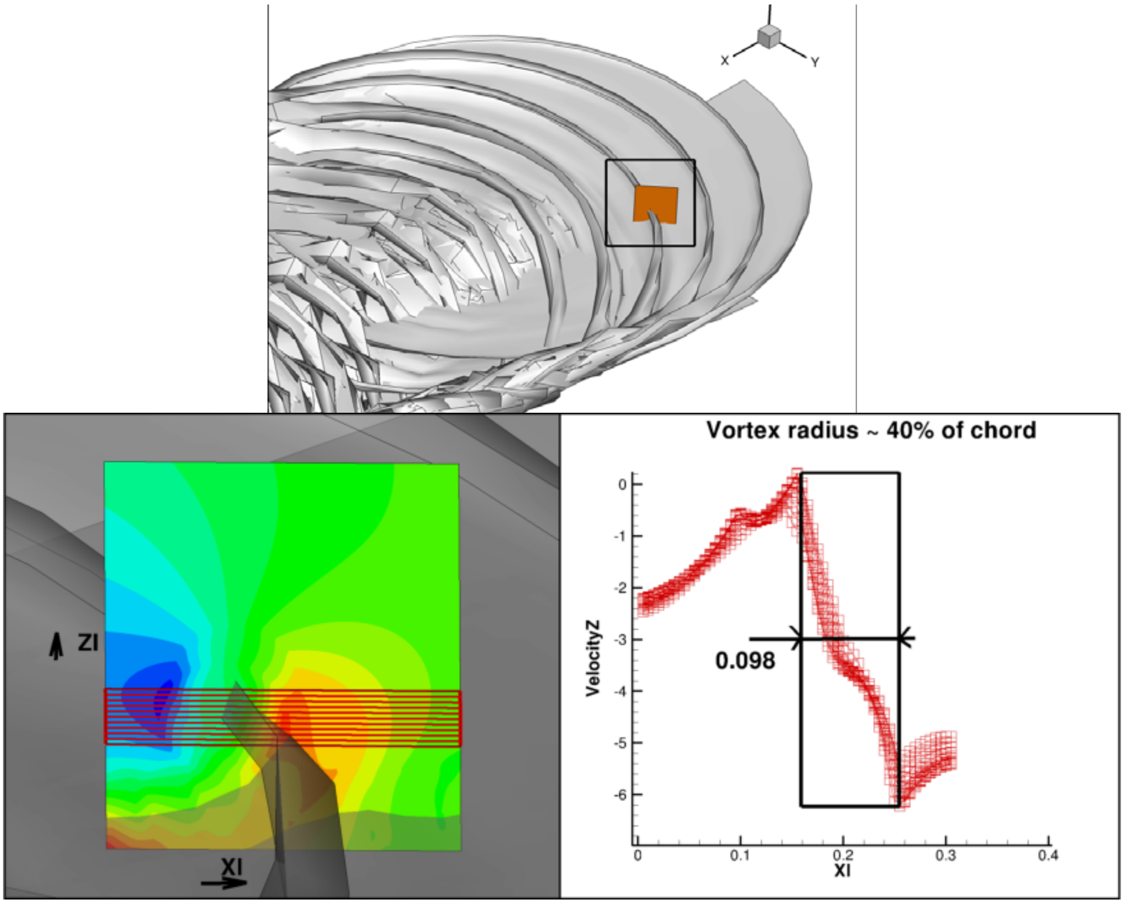

Figure 8 – Left: Contour of the velocity component along the Z axis of the induced velocity in a plane intersecting the tip vortex – Right: velocity component along Z axis is plotted for several horizontal cuts

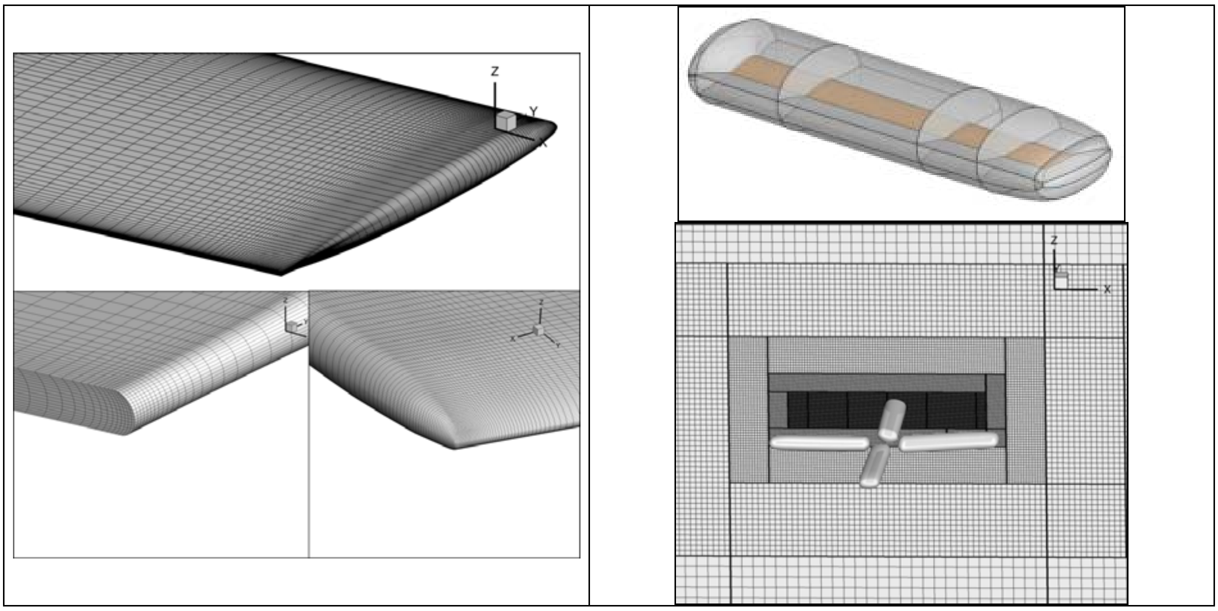

Figure 9 – 7A rotor grid – Left: view of the surface mesh at the blade tip – Right: view of the multiblock topology of the blade grid and the Cartesian background grid

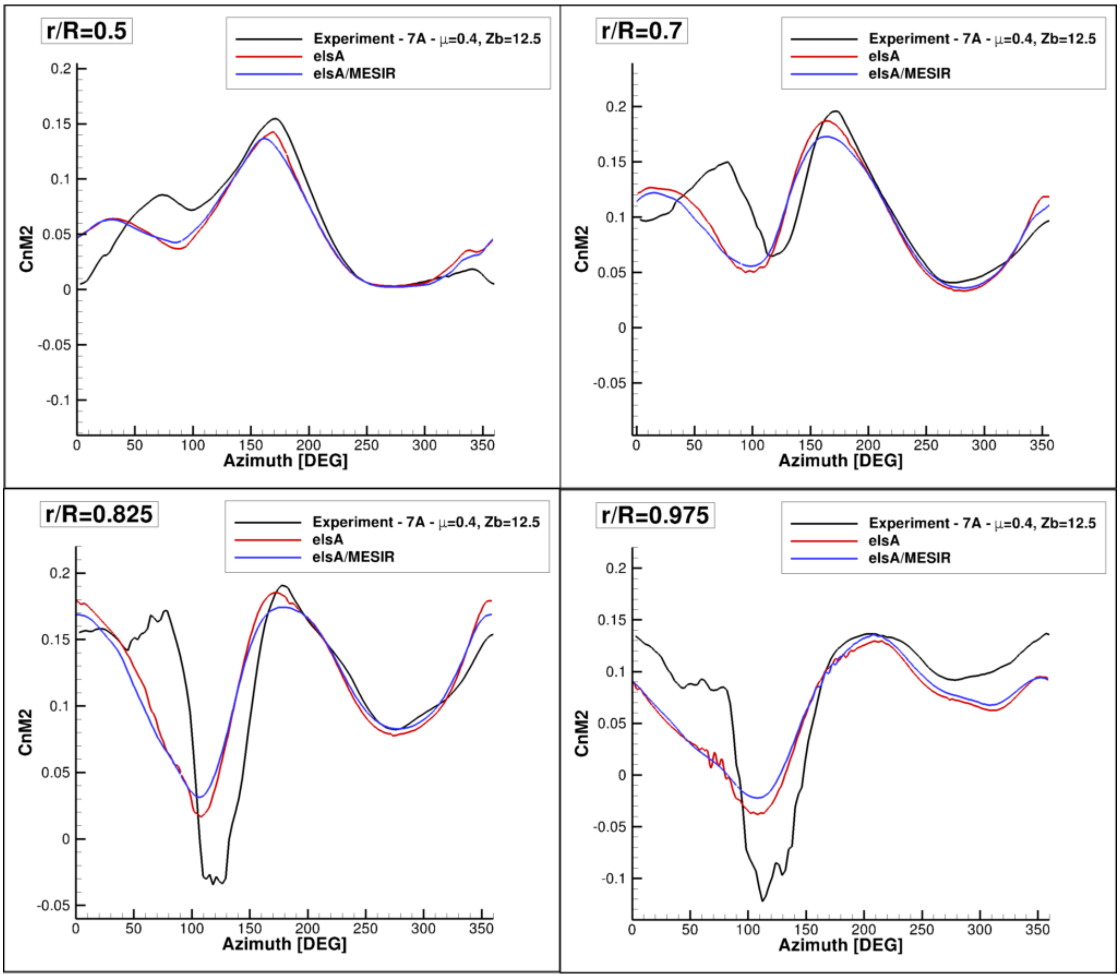

Figure 10 – Comparison of sectional normal force between experimental results, coupled Euler/Lagrange computation, full Eulerian computation

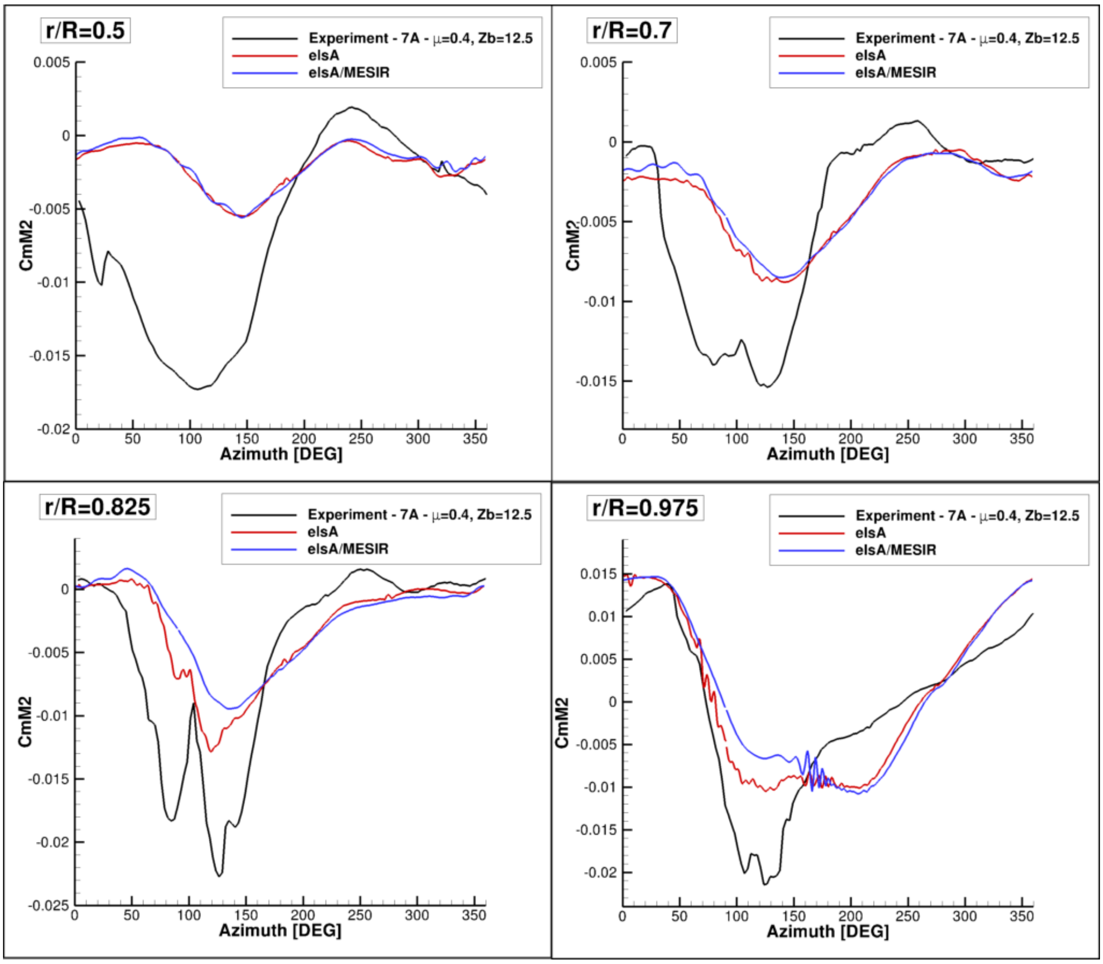

Figure 11 – Comparison of sectional pitching moment between experimental results, coupled Euler/Lagrange computation, full Eulerian computation

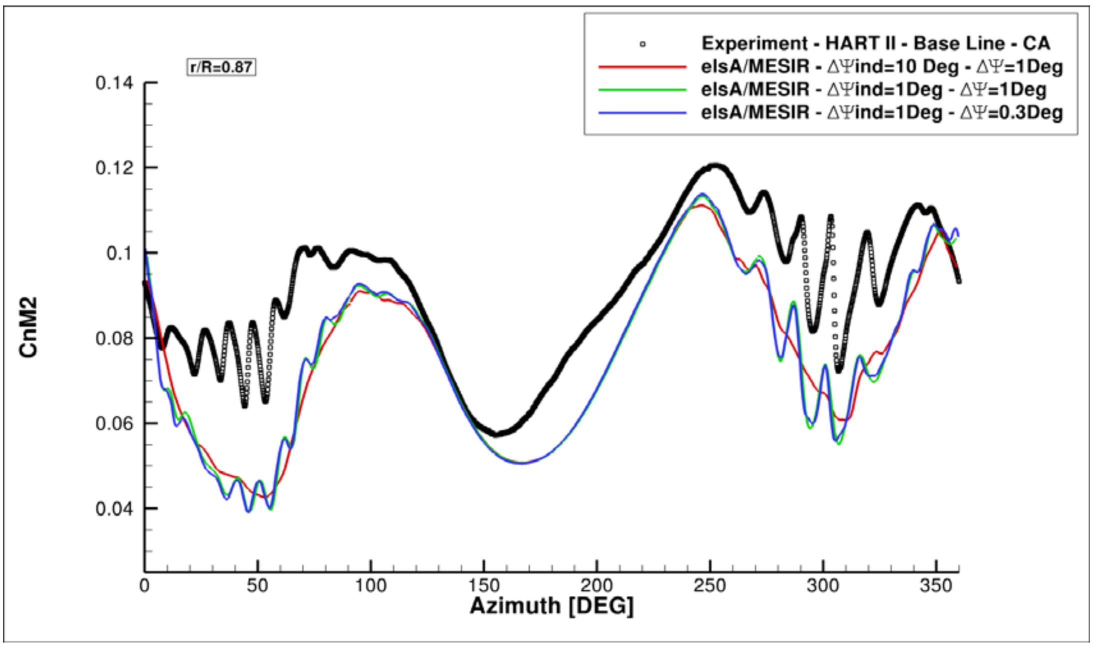

Figure 12 – Comparison of sectional normal force at r/R=0.87 between experimental results and coupled Euler/Lagrange computation – Effect of the induced velocities time step, and Eulerian computation time step

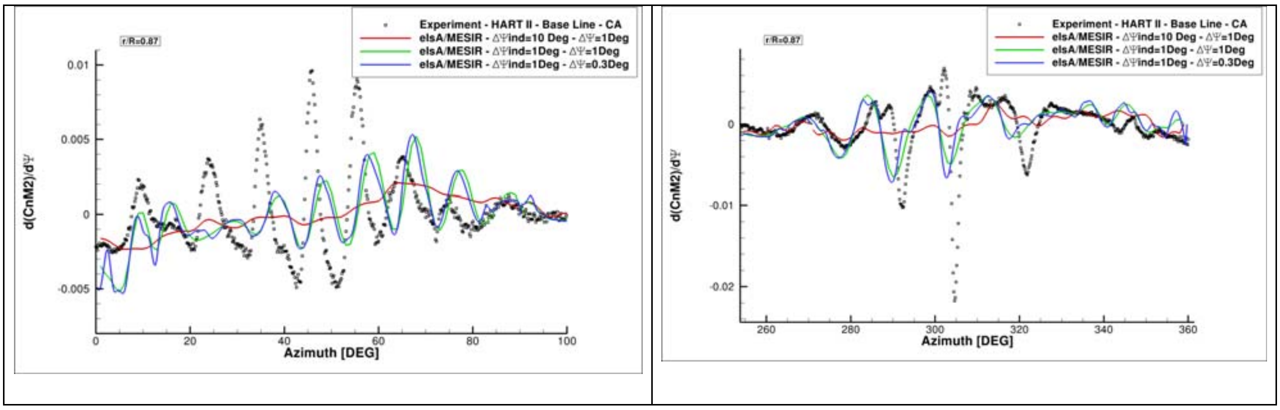

Figure 13 – Comparison of derivative of the sectional normal force at r/R=0.87 between experimental results and coupled Euler/Lagrange computation – Effect of the induced velocities time step, and Eulerian computation time step – left: advancing side – right: retreating side

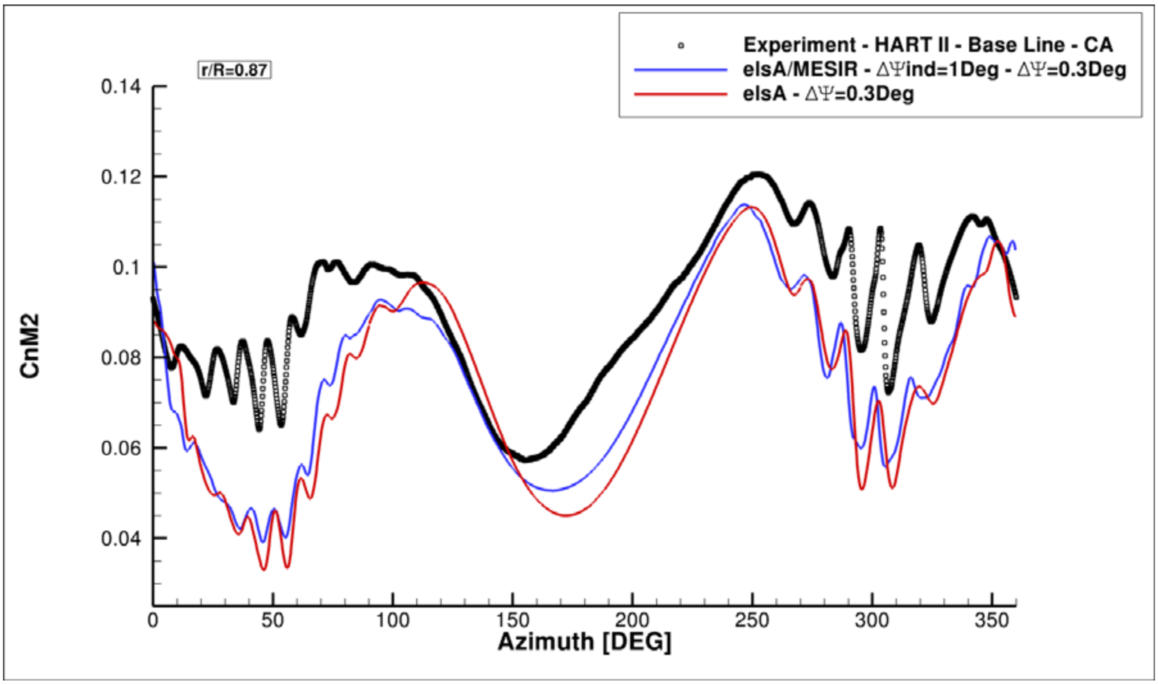

Figure 14 – Comparison of sectional normal force at r/R=0.87 between experimental results, coupled Euler/Lagrange computation and full Eulerian computation

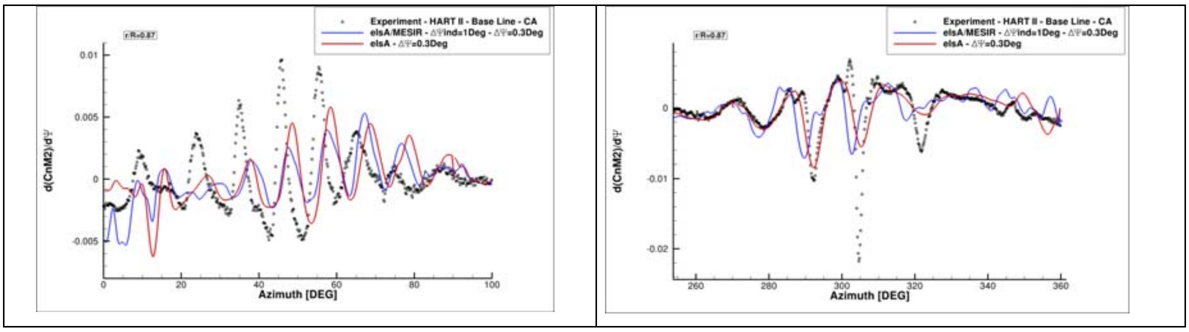

Figure 15 – Comparison of derivative of the sectional normal force at r/R=0.87 between experimental results, coupled Euler/Lagrange computation and full Eulerian computation side

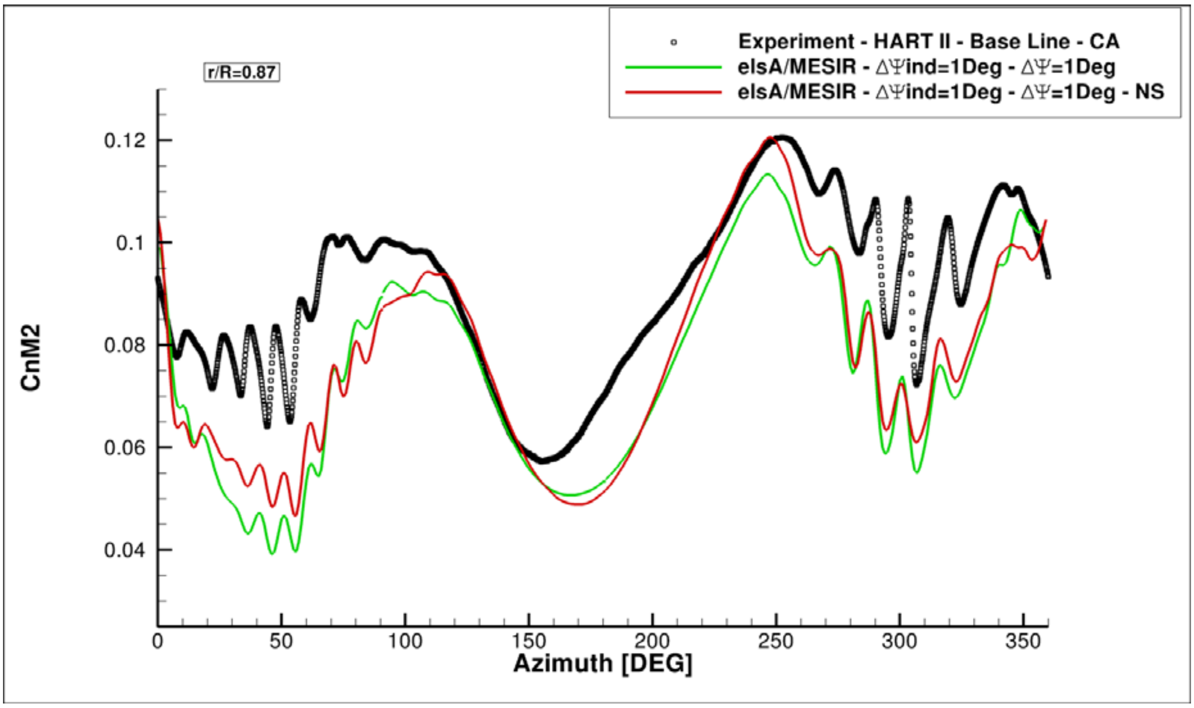

Figure 16 – Comparison of sectional normal force at r/R=0.87 between experimental results, coupled hybrid computation non viscous and viscous assumptions